Supplementary Materials for

Microcomb-driven Photonic Chip for Solving Partial Differential Equations

Hongyi Yuan[1]†, Zhuochen Du[2]†, Huixin Qi[2]†, Guoxiang Si[1]†, Cuicui Lu[1*], Yan Yang[3*], Ze Wang,[2] Bo Ni,[2,4] Yufei Wang[2], Qi-Fan Yang,[2,4,5] Xiaoyong Hu[2,4,5,6*], Qihuang Gong[2,4,5,6]

[1]*Key Laboratory of Advanced Optoelectronic Quantum Architecture and Measurements of Ministry of Education, Beijing Key Laboratory of Nanophotonics and Ultrafine Optoelectronic Systems, Center for Interdisciplinary Science of Optical Quantum and NEMS Integration, School of Physics, School of Physics, Beijing Institute of Technology, Beijing 100081, China*

[2]*State Key Laboratory for Mesoscopic Physics & Department of Physics, Collaborative Innovation Center of Quantum Matter, Beijing Academy of Quantum Information Sciences, Nano-optoelectronics Frontier Center of Ministry of Education, Peking University, Beijing 100871, China*

[3]*Institute of Microelectronics, Chinese Academy of Sciences, Beijing 100029, China.*

[4]*Peking University Yangtze Delta Institute of Optoelectronics, Nantong, Jiangsu 226010, China*

[5]*Collaborative Innovation Center of Extreme Optics, Shanxi University, Taiyuan, Shanxi 030006, China*

[6]*Hefei National Laboratory, Hefei 230088,China*

[*]E-mail: cuicuilu@bit.edu.cn; yyang10@ime.ac.cn; xiaoyonghu@pku.edu.cn

†*These authors contributed equally to this work*

This supplementary file includes:

Supplementary Note 1: Scaling Scheme for MVM based on Microring Array

The elements vectors generated in PDE solving are real but the power intensity of light is nonnegative. To solve this mismatch, a scaling operation is presented: $\boldsymbol{x} = a\boldsymbol{P} + b\boldsymbol{I}$. Here, $\boldsymbol{P}$ is power intensity vector and $\boldsymbol{I}$ is a constant vector filled with one. Factors a and b are given as below:

$$a = \frac{x_{max} - x_{min}}{P_{max} - P_{min}}, b = \frac{x_{min}P_{max} - x_{max}P_{min}}{P_{max} - P_{min}}. \quad (2)$$

Here, x_{max} and x_{min} are maximum and minimum values of the vector $\boldsymbol{x}$ while P_{max} and P_{min} are maximum and minimum of power intensity. The elements of matrixes solved with light in this work are nonnegative and transmission of drop port of a microring ranges from 0 to 1. A simple scaling operation can be applied to handle it: $R = S \cdot T$, where R is the target matrix, T is the transmission matrix of the microring array and S is a constant diagonal matrix. The diagonal elements of matrix S are maximum of each row of R divided by the maximum of the corresponding row of T. In this way, we have:

$$R \cdot \boldsymbol{x} = \boldsymbol{R}(a\boldsymbol{P} + b\boldsymbol{I}) = aS \cdot (T \cdot \boldsymbol{P}) + bR \cdot \boldsymbol{I} \quad (3)$$

Term $T \cdot \boldsymbol{P}$ is the part computed when light propagates and other operations are finished in the external controller. The time complexity of $T \cdot \boldsymbol{P}$ is $O(n^2)$ (n is vector size) which accounts for the most computation cost. During the iteration process, matrix R is constant, so the calculation of $R \cdot \boldsymbol{I}$ can be finished before iteration process of solving PDEs. The multiplication between diagonal matrix S and vector $T \cdot \boldsymbol{P}$ is simple, which counts 9 times of multiplication for input vector with 9 elements. The time complexity of looking for the maximum and minimum of the input vector $\boldsymbol{x}$ is $O(n)$ (n is the length of the vector). Based on the proposed scaling operation, the MVM calculation in real number field can be finished in the form of power intensity.

Supplementary Note 2: Design and Performance of Power Splitter.

To send input signals to different rows of rings, a 1:9 power splitter is designed, which consists of four 1:3 power splitters optimized with inverse design method based on adjoint method [48–53]. A function is used to describe the basic shape of the structure. The positions of points on the boundary are optimized according the calculated shape derivatives. The operation wavelength range is determined according to the wavelength channels selected for microring array. Here, the wavelength range is set as 1520 nm ~ 1580 nm, covering at least 3 times of free spectrum range for the designed microrings. The optimization target is to optimize the transmission of 3 output

ports to the value of 1/3 in the concerned wavelength range. The structure has a length of 7.5 μm and a width of 4 μm. The narrowest linewidth of the structure is set more than 200 nm to fulfill fabrication requirement.

The performance of the optimized structure is shown in Fig. S1(A). The structure is optimized with inverse design algorithms. The power splitter works in a bandwidth ranging from 1520 nm to 1580 nm. In the operation band, the difference of the transmission for different wavelengths is not more than 0.02. The distribution of the magnitude of electric field at wavelength of 1560 nm is shown in Fig. S1(B). It can be seen the intensity distributions of three channels are similar.

Supplementary Note 3: Fabrication Process of the Nanophotonic Chip

The chip is manufactured in a CMOS pilot line using 248 nm deep ultraviolet (DUV) photolithography for device production. All devices are fabricated on a 200 mm diameter silicon-on-insulator (SOI) wafer, featuring a 220 nm-thick top silicon layer and a 3 μm-thick buried oxide (BOX) layer. Initially, the wafer is coated with a positive photoresist and patterned using DUV lithography, followed by a double inductively coupled plasma (ICP) etching process of the top silicon. The device's waveguides are created with a full 220 nm-depth etch, while grating couplers are formed using a shallower 70 nm-depth etch. To minimize optical loss in the waveguides, a high-temperature annealing process is applied. Subsequently, a 1 μm-thick cladding silicon dioxide layer is deposited via plasma-enhanced chemical vapor deposition (PECVD), preceding the heater and metallization steps. A 55 nm-thick TiN layer is deposited using PECVD, then dry etched to form the microring heaters. An 800 nm-thick AlCu layer is deposited and selectively wet etched to create the metallization pattern. Finally, another 1 μm-thick cladding silicon dioxide layer is deposited via PECVD, followed by pad opening etching to define the wire bonding pads.

Supplementary Note 4: The Process of Packaging

First, the chip undergoes immersion in a cleaning agent solution followed by ultrasonic cleaning to ensure thorough cleaning. Next, nitrogen is used to dry the chip. The cleaned chip is then securely mounted onto a metal base and cured in an oven for stabilization. Following the circuit diagram, wire bonding techniques are employed to connect the chip to the PCB pads. The assembled product undergoes thermal curing and aging processes in an oven for comprehensive stabilization. The integrity of the chip's gold wire is carefully inspected. Finally, the product is securely packaged in a box to safeguard it during transportation.

Supplementary Note 5: Details of the Optical Frequency Comb

Kerr microcomb is generated in a high-quality-factor Si_3N_4 optical microresonator (Qaleido photonics) driven by a distributed feedback (DFB) laser. The 80 mW emission from the facet of the DFB laser chip is focused using a microlens before coupling into the bus waveguide of the Si_3N_4 chip. The output of the Si_3N_4 chip is collected using a lensed fiber. These devices are sealed in a standard butterfly package together with a thermos-optic cooler to stabilize the temperature. The single-soliton state can be deterministically accessed by turning on the driving current for the DFB laser to a preset level, known as the "turnkey" operation. The measured spectra of the optical frequency comb are shown in Fig. S2. The distance between two comb teeth is 0.8 nm.

Supplementary Note 6: Details of Measurement

The measurement is finished based on a homemade fiber-coupled microscope optical system. The chip is attached tightly on the loading platform by a suction pump. Two fiber arrays are aligned with the input and output gratings of the chip, which is shown in Fig. S2. The input port is on the left side while the output port is on the right side. The number and interval distance of the fiber array are the same as the one's of grating array. To get the fiber array aligned with the grating array of the chip, two gratings are at the start and the end of the grating array are connected directly with each other through waveguide. Injecting light from the first fiber and finely tuning the relative position between chip and fiber array, the fiber array will get aligned with the grating array when the signal from the last fiber becomes maximum.

For the measurement of the test ring, a supercontinuum laser source is connected to the input fiber array. The input grating of the microring array is aligned with one fiber in the fiber array. A telecom optical spectrum analyzer (Yokogawa AQ6370D) is used to measure the spectrum of the drop port of each row one by one.

In the demonstration of PDE solving, signal from the optical frequency comb is divided by a dense wavelength demultiplexer (DWDM) to get separated wavelength channels. The central wavelength difference of two adjacent DWDM channels is 0.8 nm. The used DWDM channels is given in table (S1). Signals of each wavelength channel are modulated by an electrically variable optical attenuator independently and then multiplexed together by the wavelength multiplexer. The modulation information on light is injected into the input gratings of chip through the input fiber array. Output light signals from the nine drop ports of microring array are measured by a set of power meters through the output fiber array.

The voltages of the electrodes are tuned manually to get the power intensity of target wavelength channels to the set value. The telecom optical spectrum analyzer is used to monitor the response of one row, and voltages of the electrodes microrings on the row are tuned. Because of the heat effects on the chip, the tuning of one row will bring influences to the adjacent row. To solve this, two loops of tuning are needed. In the first loop, coarse tuning of voltages is performed. Fine tuning of voltages of the electrodes is finished in the second loop. The spectra of the chip will be stable for a period when the heat balance is achieved inside the photonic chip.

Supplementary Note 7: Deduction of Iteration Format of Heat Equation.

The Heat equation solved in the main text is written as below:

$$\frac{\partial u}{\partial t} = a\,\nabla^2 u + q(t), -3 \le x \le 3\,,\ -3 \le y \le 3\,, \tag{1}$$

To solve this equation, finite difference method is applied to discretize the solving domain and the PDE is converted into matrix form. Time division multiplexing and matrix partition techniques are used to solve the matrix equation with our photonic chip. The equation (1) can then be written as:

$$\frac{u_{ij}^{n} - u_{ij}^{n-1}}{\Delta t} = \frac{a}{h^2}\left(u_{i+1j}^{n-1} + u_{i-1j}^{n-1} + u_{ij-1}^{n-1} + u_{ij+1}^{n-1} - 4u_{ij}^{n-1}\right) + q\,(t)\,. \tag{2}$$

In this equation, Δt is time step and h is the grid size. The matrix form of the iteration format of the equation is as below:

$$\boldsymbol{u}^{n} = \frac{\Delta t a}{h^2} A \cdot \boldsymbol{u}^{n-1} + \boldsymbol{u}^{n-1} + q\,(t)\Delta t\,. \tag{3}$$

Here, matrix A is the matrix form of Laplacian operator. Taking *n*=3 as an example, the matrix form can be written as:

$$\begin{bmatrix} u_{0,0} \\ u_{0,1} \\ u_{0,2} \\ u_{1,0} \\ u_{1,1} \\ u_{1,2} \\ u_{2,0} \\ u_{2,1} \\ u_{2,2} \end{bmatrix}^{n} = \frac{\Delta ta^{2}}{h^{2}} \begin{bmatrix} -4 & 1 & 0 & 1 & 0 & 0 & 0 & 0 & 0 \\ 1 & -4 & 1 & 0 & 1 & 0 & 0 & 0 & 0 \\ 0 & 1 & -4 & 0 & 0 & 1 & 0 & 0 & 0 \\ 1 & 0 & 0 & -4 & 1 & 0 & 1 & 0 & 0 \\ 0 & 1 & 0 & 1 & -4 & 1 & 0 & 1 & 0 \\ 0 & 0 & 1 & 0 & 1 & -4 & 0 & 0 & 1 \\ 0 & 0 & 0 & 1 & 0 & 0 & -4 & 1 & 0 \\ 0 & 0 & 0 & 0 & 1 & 0 & 1 & -4 & 1 \\ 0 & 0 & 0 & 0 & 0 & 1 & 0 & 1 & -4 \end{bmatrix} \cdot \begin{bmatrix} u_{0,0} \\ u_{0,1} \\ u_{0,2} \\ u_{1,0} \\ u_{1,1} \\ u_{1,2} \\ u_{2,0} \\ u_{2,1} \\ u_{2,2} \end{bmatrix}^{n-1} + \begin{bmatrix} u_{0,0} \\ u_{0,1} \\ u_{0,2} \\ u_{1,0} \\ u_{1,1} \\ u_{1,2} \\ u_{2,0} \\ u_{2,1} \\ u_{2,2} \end{bmatrix}^{n-1} + q(t)\Delta t \tag{4}$$

Matrix A is loaded on the microring array after removing the negative diagonal elements. The iteration format for optical solving is as below:

$$\boldsymbol{u}^{n} = \frac{\Delta ta}{h^{2}} R \cdot \boldsymbol{u}^{n-1} + \left(\frac{\Delta ta}{h^{2}} d + 1 \right) \boldsymbol{u}^{n-1} + q(t)\Delta t, \tag{5}$$

where $d = -4$. Matrix R with mesh accuracy of 3×3 is given as below:

$$R = \begin{bmatrix} 0 & 1 & 0 & 1 & 0 & 0 & 0 & 0 & 0 \\ 1 & 0 & 1 & 0 & 1 & 0 & 0 & 0 & 0 \\ 0 & 1 & 0 & 0 & 0 & 1 & 0 & 0 & 0 \\ 1 & 0 & 0 & 0 & 1 & 0 & 1 & 0 & 0 \\ 0 & 1 & 0 & 1 & 0 & 1 & 0 & 1 & 0 \\ 0 & 0 & 1 & 0 & 1 & 0 & 0 & 0 & 1 \\ 0 & 0 & 0 & 1 & 0 & 0 & 0 & 1 & 0 \\ 0 & 0 & 0 & 0 & 1 & 0 & 1 & 0 & 1 \\ 0 & 0 & 0 & 0 & 0 & 1 & 0 & 1 & 0 \end{bmatrix} \tag{6}$$

The matrix R with mesh accuracy of 6×6 is given in Fig. S3, with matrix patches marked with red squares. The spectra and power matrix loading matrix R have been given in Fig. 2(h) and (i) in the main text.

Supplementary Note 8: Deduction of Iteration Format of Wave Equation.

The Wave equation solved in the main text is written as below:

$$\frac{\partial^2 u}{\partial^2 t} = a^2 \nabla^2 u \tag{7}$$

To solve this equation, finite difference method is applied to discretize the solving domain and the PDE is converted into matrix form. Time division multiplexing and matrix partition techniques are used to solve the matrix equation with our photonic chip. The equation (7) can then be written as:

$$\frac{u_{ij}^{n} + u_{ij}^{n-2} - 2u_{ij}^{n-1}}{\Delta t^2} = \frac{a^2}{h^2}(u_{i+1j}^{n-1} + u_{i-1j}^{n-1} + u_{ij-1}^{n-1} + u_{ij+1}^{n-1} - 4u_{ij}^{n-1}) \tag{8}$$

In this equation, Δt is time step and h is the grid size. The matrix form of the iteration format of the equation is as below:

$$\boldsymbol{u}^n = \frac{\Delta t^2 a^2}{h^2} A \cdot \boldsymbol{u}^{n-1} + 2\boldsymbol{u}^{n-1} - \boldsymbol{u}^{n-2} \tag{9}$$

Matrix A is loaded on the microring array after removing the negative diagonal elements. The iteration format for optical solving is as below:

$$\boldsymbol{u}^n = \frac{\Delta t^2 a^2}{h^2} R \cdot \boldsymbol{u}^{n-1} + (2+d)\boldsymbol{u}^{n-1} - \boldsymbol{u}^{n-2} \tag{10}$$

Supplementary Note 9: Deduction of Iteration Format of Burgers Equation.

Burgers equation solved in the main text has following form:

$$\frac{\partial u}{\partial t} + u\nabla u = \nu \nabla^2 u,\ -1 < x, y < 1 \tag{11}$$

Square mesh is applied to discretize it. We apply backward difference for time domain and forward difference for the first-order derivative in space domain. Central difference is applied for the second-order derivative in space domain. The equation can be written in finite difference form as below:

$$\frac{u_{i,j}^{n}-u_{i,j}^{n-1}}{\Delta t}+u_{i,j}^{n-1}\left(\frac{u_{i+1,j}^{n-1}-u_{i,j}^{n-1}}{h}+\frac{u_{i,j+1}^{n-1}-u_{i,j}^{n-1}}{h}\right)= \nu\frac{u_{i+1,j}^{n-1}+u_{i-1,j}^{n-1}+u_{i,j+1}^{n-1}+u_{i,j-1}^{n-1}-4u_{i,j}^{n-1}}{h^2} \tag{12}$$

Here, h is the grid size and Δt is the time step. The equation can then be written in matrix format after moving the non-linear term to the right side:

$$\frac{\partial \boldsymbol{u}^{n}}{\partial t}=\frac{\nu}{h^2}A\cdot\boldsymbol{u}^{n-1}-\frac{\boldsymbol{u}^{n-1}}{h}B\cdot\boldsymbol{u}^{n-1} \tag{13}$$

Here A is the matrix form of Laplacian operator, ∇^2 , and B is the matrix form of Del operator, ∇. Taking mesh size of 3×3 as example, matrix A is given in equation (4). The matrix B is given as below:

$$B=\begin{bmatrix} -2 & 0 & 0 & 0 & 0 & 0 & 0 & 0 & 0 \\ 1 & -2 & 0 & 0 & 0 & 0 & 0 & 0 & 0 \\ 0 & 1 & -2 & 0 & 0 & 0 & 0 & 0 & 0 \\ 1 & 0 & 0 & -2 & 0 & 0 & 0 & 0 & 0 \\ 0 & 1 & 0 & 1 & -2 & 0 & 0 & 0 & 0 \\ 0 & 0 & 1 & 0 & 1 & -2 & 0 & 0 & 0 \\ 0 & 0 & 0 & 1 & 0 & 0 & -2 & 0 & 0 \\ 0 & 0 & 0 & 0 & 1 & 0 & 1 & -2 & 0 \\ 0 & 0 & 0 & 0 & 0 & 1 & 0 & 1 & -2 \end{bmatrix} \tag{14}$$

The matrixes can be loaded on the microring array after removing the negative diagonal elements. The iteration format for optical solving can then be written as below:

$$\frac{\partial \boldsymbol{u}^{n}}{\partial t}=\frac{\nu}{h^2}\left(R_1\cdot\boldsymbol{u}^{n-1}+d_1\cdot\boldsymbol{u}^{n-1}\right)-\frac{\boldsymbol{u}^{n-1}}{h}\left(R_2\cdot\boldsymbol{u}^{n-1}+d_2\cdot\boldsymbol{u}^{n-1}\right)=f(\boldsymbol{u}^{n-1}) \tag{15}$$

Here, $d_1=-4$ and $d_2=-4$. The iteration format for Burgers equation is given as below:

$$\boldsymbol{u}^{n}=f(\boldsymbol{u}^{n-1})\cdot\Delta t+\boldsymbol{u}^{n-1}, \tag{16}$$

where $f(\boldsymbol{u}^{n-1})$ has been given in (15). Two terms of the matrix vector multiplication $R_1\cdot\boldsymbol{u}^{n-1}$ and $R_2\cdot\boldsymbol{u}^{n-1}$ are performed through the photonic chip, which account for the most in the solving process because other terms can be regarded as simply multiplying and adding a constant number. Coefficient matrix of Laplacian operator of Burgers equation is as below:

$$R_1 = \begin{bmatrix} 0 & 1 & 0 & 1 & 0 & 0 & 0 & 0 & 0 \\ 1 & 0 & 1 & 0 & 1 & 0 & 0 & 0 & 0 \\ 0 & 1 & 0 & 0 & 0 & 1 & 0 & 0 & 0 \\ 1 & 0 & 0 & 0 & 1 & 0 & 1 & 0 & 0 \\ 0 & 1 & 0 & 1 & 0 & 1 & 0 & 1 & 0 \\ 0 & 0 & 1 & 0 & 1 & 0 & 0 & 0 & 1 \\ 0 & 0 & 0 & 1 & 0 & 0 & 0 & 1 & 0 \\ 0 & 0 & 0 & 0 & 1 & 0 & 1 & 0 & 1 \\ 0 & 0 & 0 & 0 & 0 & 1 & 0 & 1 & 0 \end{bmatrix} \tag{17}$$

The coefficient matrix of Del operator is given as below:

$$R_2 = \begin{bmatrix} 0 & 0 & 0 & 0 & 0 & 0 & 0 & 0 & 0 \\ 1 & 0 & 0 & 0 & 0 & 0 & 0 & 0 & 0 \\ 0 & 1 & 0 & 0 & 0 & 0 & 0 & 0 & 0 \\ 1 & 0 & 0 & 0 & 0 & 0 & 0 & 0 & 0 \\ 0 & 1 & 0 & 1 & 0 & 0 & 0 & 0 & 0 \\ 0 & 0 & 1 & 0 & 1 & 0 & 0 & 0 & 0 \\ 0 & 0 & 0 & 1 & 0 & 0 & 0 & 0 & 0 \\ 0 & 0 & 0 & 0 & 1 & 0 & 1 & 0 & 0 \\ 0 & 0 & 0 & 0 & 0 & 1 & 0 & 1 & 0 \end{bmatrix}. \tag{18}$$

In Fig. S4, we plot the matrix R_2 for mesh size of 6×6, with matrix patches marked with red squares.

Supplementary Note 10: The Loading of the Coefficient Matrix of Burgers Equation.

The loading of the two operators deducted in the former section is given here. The top left part of the coefficient matrixes of two operators are given in Fig. S5(a). The measured normalized spectra of the microring array with optical frequency comb as light source is given in Fig. S5(b). The normalized power matrix measured with power meters is shown in Fig. S5(c). These results show that the coefficient matrix of Burgers equation is loaded on the photonic chip successfully, which promise the correctness of later PDE solving.

Supplementary Note 11: Solving Results with Super Continuous Laser Source

Here, the solving results of Heat equation with super continuous laser source (SCLS) is provided to prove the advantages of using optical frequency comb in the photonic solving of PDEs. The signal from SCLS is a continuous spectrum, which is divided with DWDM to generate

independently tunable signal channels. Every two adjacent wavelength channels are separated by a DWDM channel to reduce crosstalk. The solving process is described in the manuscript. The solving results are presented in Fig. S6. Comparing the results solved using optical frequency comb in Fig. 3(a)-(h), the error in the results using SCLS is much bigger. This proves the advantages of optical frequency comb in solving PDEs. The optical frequency comb provides equidistant signal peaks with high signal to noise ratio and low crosstalk, which makes the loading of matrix patches more accurate.

Supplementary Note 12: Deduction of Iteration Format of Poisson equation.

To solve Poisson equation numerically, square mesh is applied to discretize the solving area. The general form of Poisson equation is as followed:

$$\frac{\partial^2 u}{\partial^2 x}+\frac{\partial^2 u}{\partial^2 y}=f(x,y),-3\le x\le 3,\ -3\le y\le 3. \tag{19}$$

When the term on the right side is zero, the equation becomes Laplace's equation. The equation can be written in finite difference form:

$$\frac{u_{i+1,j}+u_{i,j+1}-4u_{i,j}+u_{i-1,j}+u_{i,j-1}}{h^2}=f(x,y),i,j=0,1,2\cdots\cdots n-1. \tag{20}$$

Here, indexes i,j denote the function value defined on the grid points within the solving area. The number n is the grid number. The mesh size is h. The discretized equation can be further written in matrix form. Taking n=3 as an example, the matrix form is:

$$\begin{bmatrix} -4 & 1 & 0 & 1 & 0 & 0 & 0 & 0 & 0 \\ 1 & -4 & 1 & 0 & 1 & 0 & 0 & 0 & 0 \\ 0 & 1 & -4 & 0 & 0 & 1 & 0 & 0 & 0 \\ 1 & 0 & 0 & -4 & 1 & 0 & 1 & 0 & 0 \\ 0 & 1 & 0 & 1 & -4 & 1 & 0 & 1 & 0 \\ 0 & 0 & 1 & 0 & 1 & -4 & 0 & 0 & 1 \\ 0 & 0 & 0 & 1 & 0 & 0 & -4 & 1 & 0 \\ 0 & 0 & 0 & 0 & 1 & 0 & 1 & -4 & 1 \\ 0 & 0 & 0 & 0 & 0 & 1 & 0 & 1 & -4 \end{bmatrix} \cdot \begin{bmatrix} u_{0,0} \\ u_{0,1} \\ u_{0,2} \\ u_{1,0} \\ u_{1,1} \\ u_{1,2} \\ u_{2,0} \\ u_{2,1} \\ u_{2,2} \end{bmatrix} = \begin{bmatrix} h^2 f_{0,0}-u_{-1,0}-u_{0,-1} \\ h^2 f_{0,1}-u_{-1,1} \\ h^2 f_{0,2}-u_{-1,2}-u_{0,3} \\ h^2 f_{1,0}-u_{1,-1} \\ h^2 f_{1,1} \\ h^2 f_{1,2}-u_{1,3} \\ h^2 f_{2,0}-u_{2,-1}-u_{3,0} \\ h^2 f_{2,1}-u_{3,1} \\ h^2 f_{2,2}-u_{2,3}-u_{3,2} \end{bmatrix}. \tag{21}$$

The matrix on the left side of the equation contains the relationship between grid points determined by the Laplacian operator in the PDE equation. The vector multiplied with the matrix is the variables to be solved. The vector on the right side contains the source term, $f(x,y)$, of the PDE equation and boundary values which have indexes of -1 or 3. The matrix equation above has the form of $A\boldsymbol{X}=\boldsymbol{B}$, which can be solved with Jacobi iteration method in an iteration style [47]:

$$\boldsymbol{X}^{(k+1)} = D^{-1}(\boldsymbol{B} - M\boldsymbol{X}^{(k)}), D = diag(A), M = A - diag(A). \tag{22}$$

where $D = -4I$ and I is identity matrix. The iteration equation can be further simplified as:

$$\boldsymbol{X}^{(k+1)} = \boldsymbol{C} + R \cdot \boldsymbol{X}^{(k)}, C = \frac{\boldsymbol{B}}{d}, R = -\frac{M}{d}, d = -4. \tag{23}$$

The deduction above suitable for diagonally dominant PDE problems which are widely concerned in various scientific and engineering situations [61]. The coefficient matrix, *R*, is given as below:

$$R = 1/4 \begin{bmatrix} 0 & 1 & 0 & 1 & 0 & 0 & 0 & 0 & 0 \\ 1 & 0 & 1 & 0 & 1 & 0 & 0 & 0 & 0 \\ 0 & 1 & 0 & 0 & 0 & 1 & 0 & 0 & 0 \\ 1 & 0 & 0 & 0 & 1 & 0 & 1 & 0 & 0 \\ 0 & 1 & 0 & 1 & 0 & 1 & 0 & 1 & 0 \\ 0 & 0 & 1 & 0 & 1 & 0 & 0 & 0 & 1 \\ 0 & 0 & 0 & 1 & 0 & 0 & 0 & 1 & 0 \\ 0 & 0 & 0 & 0 & 1 & 0 & 1 & 0 & 1 \\ 0 & 0 & 0 & 0 & 0 & 1 & 0 & 1 & 0 \end{bmatrix} \tag{24}$$

When the mesh size of the grid is set as $3m \times 3m$ (m is integer bigger than 1), the coefficient matrix is similar, which consists of 4 non-zero patches. The coefficient matrix when mesh size is 6×6 has been given in Fig. S3. The number 1/4 is omitted because it can be multiplied after the matrix vector multiplication operation.

Supplementary Note 13: The Voltages Added in Experiment

Here, the examples of raw data of the voltages added on the electrodes to solve the PDEs in experiment is provided, which is plotted in Fig. S6. The value in x axis represents the column number and the that in y axis represents the row number of the microring array. Fig. S6(a) to (c) correspond to the solving of Poisson equation, the solving of Burgers equation, and parallel solving of PDEs, respectively. Because Heat equation, Wave equation and Laplace's equation share the same coefficient matrix with Poisson equation in this work, their voltage distributions are similar and omitted here. It should be noticed that because of the random heat fluctuation from environment, the voltages added for the same solving tasks can be different. In the experiment, different microrings have different responses to the added voltage, which can be attributed to fabrication deviations. Because of the quick heat dissipation of the rings on the boundary of the microring array, the voltages needed for them are practically larger than the average. This explains why the voltages added on rings in the first row are larger than other rows.

Supplementary Note 14: Discussion of the Photonic Solving Time of PDEs

To make a meaningful comparison of our photonic computing system with the state-of-art GPU system, it is necessary to assume that the PDE solving algorithm and external controlling system are the same. Thus, the comparison is concentrated on the MVM computation in the PDE solving process. The time cost of light propagating in our photonic chip is $L/(n_{Si}c) = 3.5\ mm/(3.45 \times 299792458 m/s) \approx 3.38$ ps. Here, L is the waveguide length between the input port and output port, n_{Si} is the refractive index of silicon waveguide around the wavelength of 1550 nm, and c is the speed of light in vacuum. Thus, the time cost of photonic computing of one time of matrix vector multiplication is about 17.92 ps. On the other hand, the core frequency of the state-of-art GPU, NVIDIA GeForce RTX 4090, is 2.28 GHz. Considering the multicore architecture of RTX 4090, we assume that one time of matrix vector multiplication computing is finished in 2 cycles of clock (multiplying and adding count one cycle for each of them). Thus, the time cost of one time of matrix vector multiplication is approximately 0.88 ns, which is much slower than our photonic system.

To compare our photonic system with the state-of-art GPU, a table about the approximated time cost of different PDEs is given in table (S2). The solving time here refers to the MVM time cost, because the external process is assumed the same for two systems. The MVM time for a given PDE is estimated by multiplying the number of times of MVM computing and the time cost for one time of MVM.

Supplementary Note 15: Time Cost and Energy Consumption of the Experimental System

The time cost of the experimental system mainly originates from the interaction between the photonic chip and controlling computer. The controlling computer sends value to the via RS232 serial communication protocol. The measured time cost for VOA to receive a value is about 13ms, which includes the time for CPU sending value in cache to serial port, data transmission time, and digital-to-analog conversion (DAC). InGaAs photodiode is used in experiment to convert optical signal to electrical current, which has a response time about 1μs. The power meter converts the analog signal to digital signal and sends it to controlling computer through USB 2.0 communication protocol. The measured time cost for the computer to read out a value from a

power meter is about 1 ms. A multi-channel variable optical attenuator (VOA) module based on micro-electro-mechanical system is used to modulate signals, which has a response time of 2ms. The controlling process is finished with a commercial desktop computer loaded with a CPU of Intel(R) Core (TM) i5-1135G7 @ 2.40GHz. The process time is about 1ns as measured. The light propagation time in the chip is about 3.38ps as estimated by dividing the chip length with light speed. Thus, the time cost of one time of matrix vector multiplication (MVM) in our experimental system is about 13ms+1μs+1ms+2ms+1ns+3.38ps≈16ms. To further reduce the time cost of the experimental system, several methods can be used. First, if the 100 GHz $LiNbO_3$ Modulators are employed [65-67], the time used to load an input vector is about 10 ps. If the high-speed InGaAs photon detectors over 220 GHz are used [68], the time cost on reading the output vector is about 4.54 ps. Second, the most advanced ADC with sampling rate of 42GS/s [69] and DAC with sampling rate of 20.48 GS/s (DAC39RFS10, Texas Instruments) can also be used. The ADC/DAC time cost will be reduced to about 30 ns. Finally, the most advanced USB4 2.0 version protocol can reach a high data transmission speed of 80Gb/s, which means the interaction time between the controlling computer and the ADC/DAC can be reduced to 2ns.

The energy consumption of the optical frequency comb is about 6.5W, including the distributed feedback laser used to pump the optical comb and the temperature controlling module. To compensate the insertion loss, an erbium-doped optical fiber amplifier is used, which has an energy consumption about 20W. The energy consumption of the VOA module is less than 1W. The energy consumption of a power meter headed with a photodiode is 1W. Because 9 power meters are used for the nine output optical channels, the energy consumption for light detection is 9W. To load matrix on the photonic chip, a 512-channel electrically tunable module is used to provide voltage ranging from 0V to 10V for each electrical wire, which has an energy consumption about 20W. The controlling computer has an energy consumption about 100W. To sum up, the energy consumption of our experimental system is about 156.5W. To further reduce the energy consumption of the experimental system, future efforts should be made from design and fabrication. For example, heterogeneous integration technology can integrate different components with different function and material on one chip, which can further reduce the energy consumption of the computing system [59].

Supplementary Note 16: Comparison Table of Optical Solving of Equation.

We provide a table (S2) below comparing the main progress in the area optical solving of equation. It is obvious that the mesh accuracy of optical solving of PDEs is not more than 5×5 in previous works. The solved PDE type is limited to Poisson equation and the parallel solving of different PDEs has never been reported before this work. This work achieves solving different types of PDEs with high mesh accuracy and performs parallel solving of PDEs in one chip, which shows our scheme is advantageous.

In addition, a figure comparing the grid number solved in the works about solving equation is also plotted in Fig. S7. We can see the realized solving grid number in this work is five times higher than that in reported works.

Supplementary Note 17: Extension of the Scheme.

Our scheme can be further extended to handle more tasks. By adding more rings in the microring array, the number of PDEs that can be solved parallelly will increase. Keeping the detailed parameters of current structures unchanged, the size of the microring array can be extended to 9×18. As demonstrated in the main text, there are four unique non-zero patches for Poisson equation, so solving a Poisson equation problem takes 9×4 rings. Therefore, a microring array with size of 9×18 can support at least the parallel solving of 4 PDEs. If more chips are connected to work together, higher computation power can be achieved. For example, two chips containing 9×9 can also be used to solve 4 PDEs parallelly. More chips can support more PDEs solved parallelly, which is demonstrated in Fig. S8. Therefore, our scheme provides a general idea to solve PDEs.

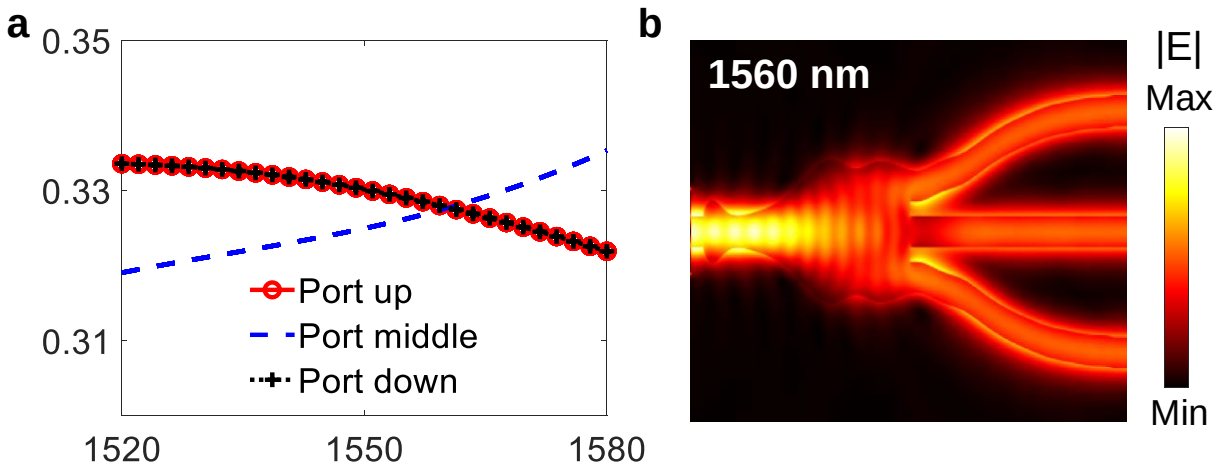

Fig. S1: Simulation Performance of Optimized Power Splitter.

The simulation performance of 3 channel power splitter. (a), the transmission of three ports. (b), the distribution of the norm of electric field at wavelength of 1560 nm.

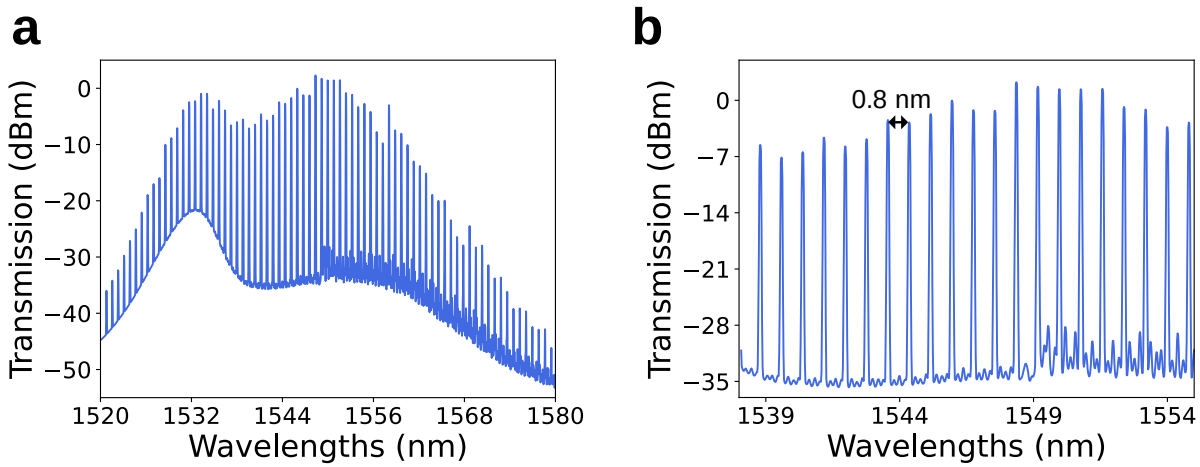

Fig. S2: Measured Spectra of Optical Comb.

(a), the spectrum of the optical comb from 1520 nm to 1580 nm; (b), the spectrum of the optical comb around 1550 nm. The distance between two adjacent teeth is 0.8 nm.

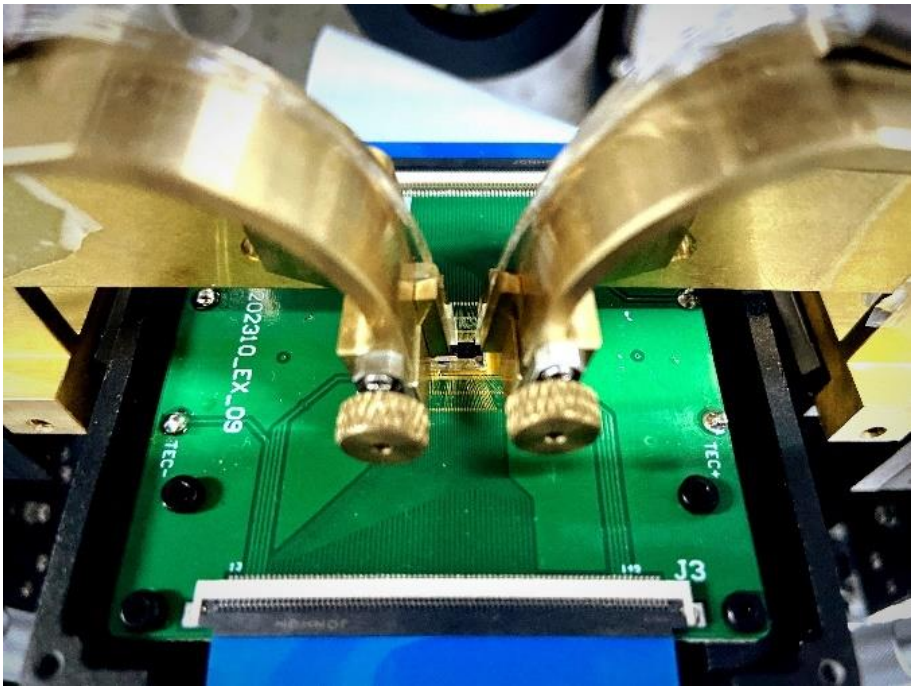

Fig. S3: The Platform for Measurement

The packaged chip is attached tightly on the loading platform. Input (left) and output (right) fiber arrays are protected by glass cladding and are caught by the metal fiber clamps.

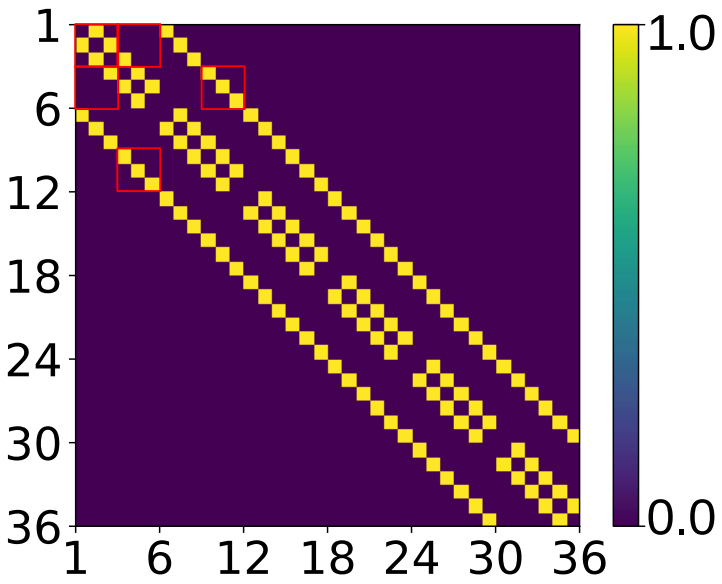

Fig. S4: The Coefficient Matrix for Laplacian Operator

The coefficient matrix for Laplacian Operator with diagonal elements removed and the mesh size is 6×6. Matrix patches denoted with red squares.

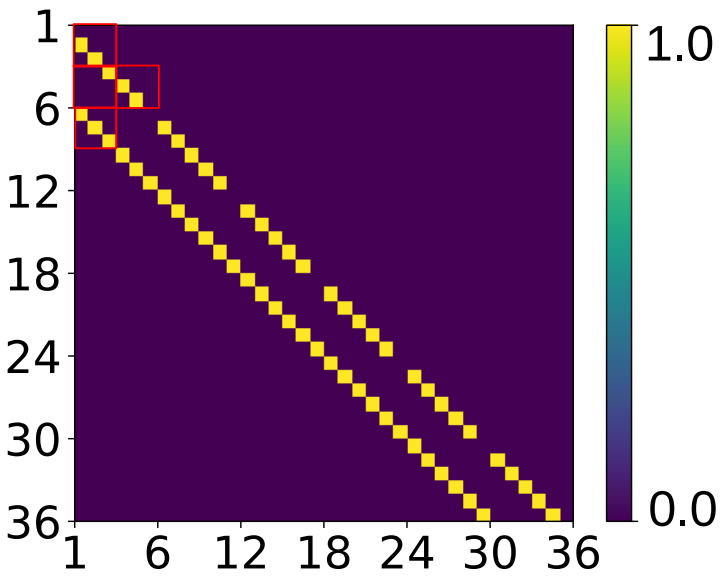

Fig. S5: The Coefficient Matrix of Del Operator

The coefficient matrix for Del operator in Burgers equation when mesh size is 6×6, with matrix patches denoted with red squares. The duplicated diagonal elements are removed.

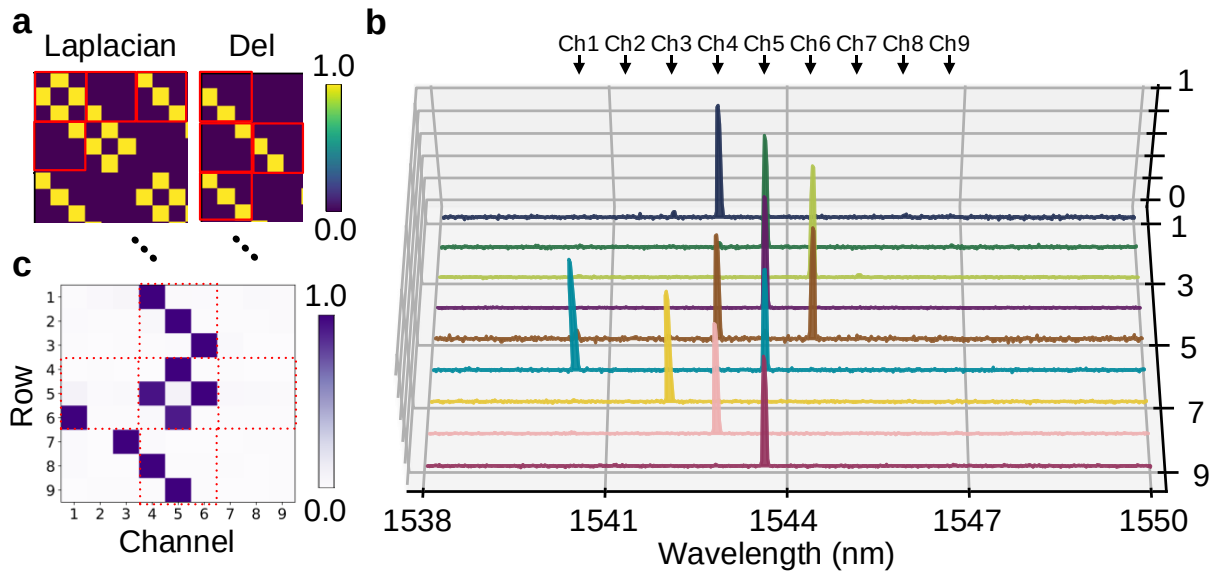

Fig. S6: The Loading of the Coefficient Matrix of Burgers Equation

(a), The top left part of the coefficient matrix of Laplacian operator and Del operator with mesh size of 6×6. Matrix patches are marked by red squares. (b), The measured normalized spectra of nine rows of the microring array with nine DWDM wavelength channels opened. The central wavelengths of nine channels are marked with arrows on the top of the figure. (c), The measured normalized power matrix of the microring array.

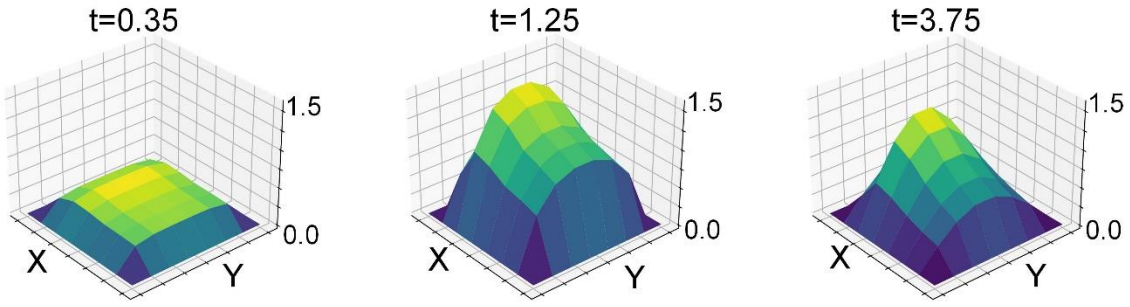

Fig. S7: Solving Results of Heat Equation with Super Continuous Laser Source

The solving results of Heat equation at different time points. It can be seen there is much more error than the results presented in the manuscript using optical comb.

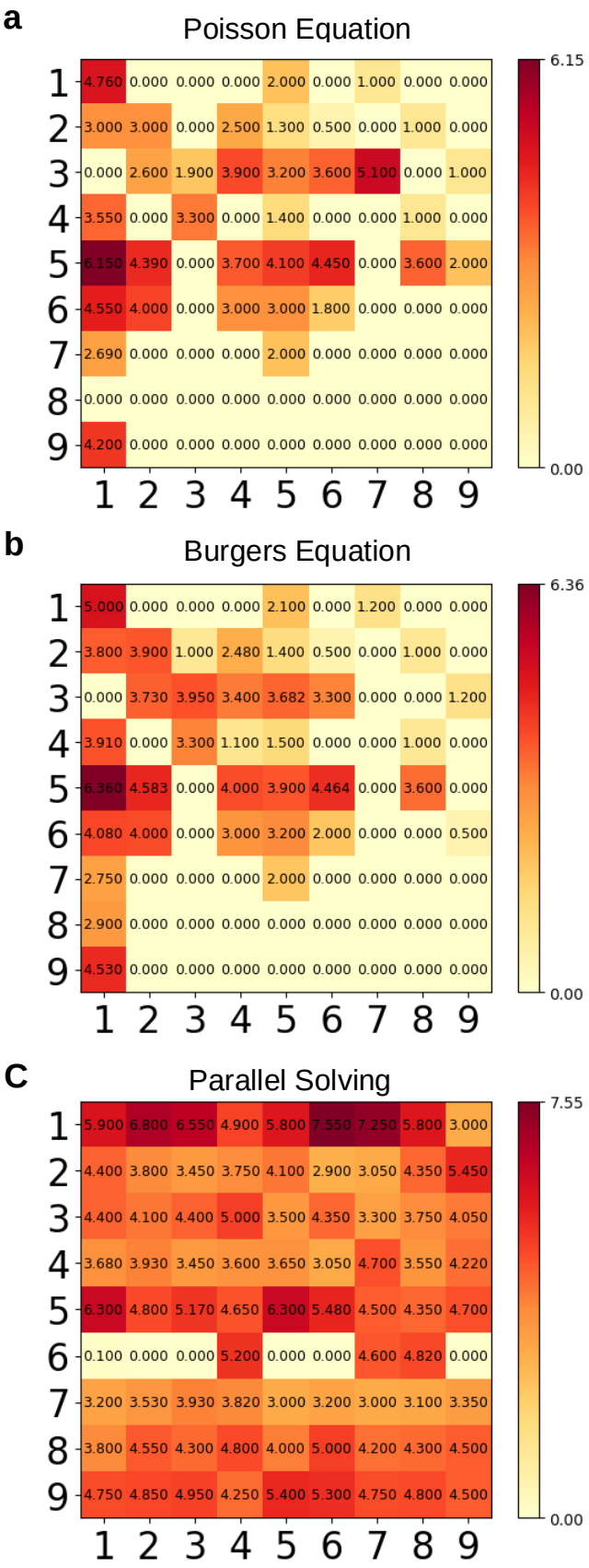
a
Poisson Equation
4.760 0.000 0.000 0.000 2.000 0.000 1.000 0.000 0.000
3.000 3.000 0.000 2.500 1.300 0.500 0.000 1.000 0.000
0.000 2.600 1.900 3.900 3.200 3.600 5.100 0.000 1.000
3.550 0.000 3.300 0.000 1.400 0.000 0.000 1.000 0.000
6.150 4.390 0.000 3.700 4.100 4.450 0.000 3.600 2.000
4.550 4.000 0.000 3.000 3.000 1.800 0.000 0.000 0.000
2.690 0.000 0.000 0.000 2.000 0.000 0.000 0.000 0.000
0.000 0.000 0.000 0.000 0.000 0.000 0.000 0.000 0.000
4.200 0.000 0.000 0.000 0.000 0.000 0.000 0.000 0.000
1 2 3 4 5 6 7 8 9
6.15
0.00
b
Burgers Equation
5.000 0.000 0.000 0.000 2.100 0.000 1.200 0.000 0.000
3.800 3.900 1.000 2.480 1.400 0.500 0.000 1.000 0.000
0.000 3.730 3.950 3.400 3.682 3.300 0.000 0.000 1.200
3.910 0.000 3.300 1.100 1.500 0.000 0.000 1.000 0.000
6.360 4.583 0.000 4.000 3.900 4.464 0.000 3.600 0.000
4.080 4.000 0.000 3.000 3.200 2.000 0.000 0.000 0.500
2.750 0.000 0.000 0.000 2.000 0.000 0.000 0.000 0.000
2.900 0.000 0.000 0.000 0.000 0.000 0.000 0.000 0.000
4.530 0.000 0.000 0.000 0.000 0.000 0.000 0.000 0.000
1 2 3 4 5 6 7 8 9
6.36
0.00
C
Parallel Solving
5.900 6.800 6.550 4.900 5.800 7.550 7.250 5.800 3.000
4.400 3.800 3.450 3.750 4.100 2.900 3.050 4.350 5.450
4.400 4.100 4.400 5.000 3.500 4.350 3.300 3.750 4.050
3.680 3.930 3.450 3.600 3.650 3.050 4.700 3.550 4.220
6.300 4.800 5.170 4.650 6.300 5.480 4.500 4.350 4.700
0.100 0.000 0.000 5.200 0.000 0.000 4.600 4.820 0.000
3.200 3.530 3.930 3.820 3.000 3.200 3.000 3.100 3.350
3.800 4.550 4.300 4.800 4.000 5.000 4.200 4.300 4.500
4.750 4.850 4.950 4.250 5.400 5.300 4.750 4.800 4.500
1 2 3 4 5 6 7 8 9
7.55
0.00

Fig. S8: The Voltage Examples Added in Experiment

This figure gives the voltage examples added on the electrodes in different solving tasks. The x axis is the column number and the y axis is the row number of the microring array. (a) to (c) correspond to the solving of Poisson equation, the solving of Burgers equation, and parallel solving of PDEs.

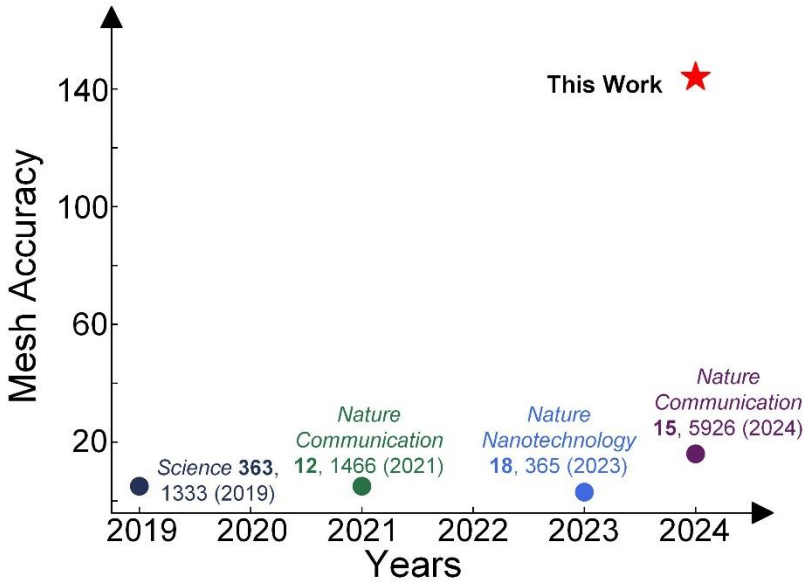

Fig. S9: The Comparison of Different Works in Equation Solving

The comparison of different works in equation solving. Here, the mesh accuracy refers to the solving point number after discretization of the equation.

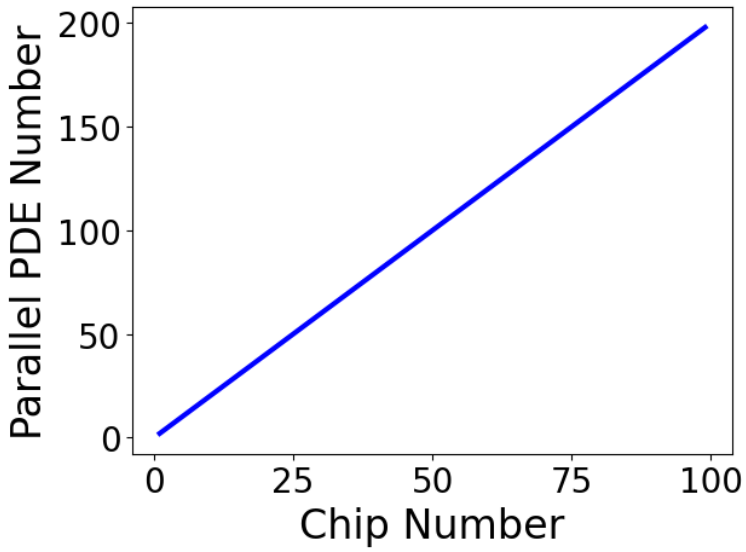

Fig. S10: Extension for PDE Parallel Solving

This figure demonstrates that more PDEs can be solved parallelly by driving more chips working together.

Table S1: The Central Wavelengths of the Used DWDM Channels

Channel Name	C38	C39	C40	C41	C42	C43	C44	C45	C46
Central Wavelength (nm)	1546.924	1546.114	1545.328	1544.545	1543.743	1542.951	1542.145	1541.367	1540.551

Table S2: The Solving Time of PDEs for Our Photonic System and GPU

	Heat Equation (mesh size: 6×6; iteration number: 200)	Wave Equation (mesh size: 6×6; iteration number: 200)	Burgers Equation (mesh size: 9×9; iteration number: 30)	Poisson Equation (mesh size: 12×12; iteration number: 10)	Laplace's Equation (mesh size: 9×9; iteration number: 10)
GPU	8712×880ps≈ 7666.6 ns	8712×880ps≈ 7666.6 ns	5220×880ps≈ 4593.6 ns	2080×880ps≈ 1830.4 ns	1110×880ps≈ 976.8 ns
Photonic Computing	8712×3.38ps ≈29.4 ns	8712×3.38ps ≈29.4 ns	5220×3.38ps ≈17.6 ns	2080×3.38ps ≈7.0 ns	2080×3.38ps ≈3.7 ns

Table S3: Comparison of Different Works of Photonic Computing

Works	Function	Mesh Accuracy	Parallel Computing	Platform	Footprint	Light Source
Science **363**, 1333 (2019)	Solving Integral Equation	5	N	Microwave Photonics	~610× 305mm^2	Monochromatic electromagnetic fields
Nature **589**, 52 (2021)	Convolution	NA	Y	Silicon Nitride Nanophotonic Chip	~6.5 × 6.5 mm^2	Optical Comb
Nature Commun. **12**, 1466 (2021)	Solving Integral Equation	5	Y	Microwave Photonics	~900× 600mm^2	Electromagnetic waves at microwave frequencies
Nature Commun. **13**, 1713 (2022)	Solving Differential Equation	NA	Y	Metasurface	Meter scale	Microwave frequencies
Nature Nanotechnol. **18**, 365 (2023)	Solving Integral Equation	3	N	Meta-gratings	NA	706nm laser
Nature Photon. **17**, 1080 (2023)	High-dimensional photonic in-memory computing	NA	Y	Silicon Nanophotonic Chip	~2 × 2 mm^2	Supercontinuum Laser
Nature **627**, 80 (2024)	Solving Ordinary Differential Equations	NA	N	Lithium Niobate Microwave Photonic Chip	~8107.3 mm^2	CW Laser
Nature Commun. **15**, 5926 (2024)	Integral Equation and Poisson Equation	4×4	N	Silicon Nitride Nanophotonic Chip	4.4 × 9.8 mm^2	CW Laser
This work	**Heat equation, Wave equation, Burgers equation, Poisson equation, and Laplace's equation**	**3×n×3×n (n>=3)**	**Y**	**Silicon Photonic Chips**	**3.7 × 2.5 mm^2**	**Optical Comb**

Y/N: Yes or No;
NA: Not applicable or not provided;
Mesh Accuracy: The solving grid number for solving equations.